



ELSEVIER

Physica C 357–360 (2001) 903–913

PHYSICA C

www.elsevier.com/locate/physc

Recent progress in the fabrication of high- J_c tapes by epitaxial deposition of YBCO on RABiTS

A. Goyal^{a,*}, D.F. Lee^a, F.A. List^a, E.D. Specht^a, R. Feenstra^a,
M. Paranthaman^a, X. Cui^b, S.W. Lu^c, P.M. Martin^a, D.M. Kroeger^a,
D.K. Christen^a, B.W. Kang^a, D.P. Norton^d, C. Park^e, D.T. Verebelyi^b,
J.R. Thompson^a, R.K. Williams^a, T. Aytug^a, C. Cantoni^a

^a *Metals and Ceramics Division, Oak Ridge National Laboratory, P.O. Box 2008, MS 6116, Oak Ridge, TN 37831-6116, USA*

^b *American Superconductor Corporation, Two Technology Drive, Westborough, MA 01581, USA*

^c *Information Products Inc., 414 East 40th Street, Holland, MI 49423, USA*

^d *University of Florida, P.O. Box 116400, Gainesville, FL 32611, USA*

^e *IGC Super Power, 450 Duane Avenue, Schenectady, NY 12304, USA*

Received 16 October 2000; accepted 21 November 2000

Abstract

Progress made in the fabrication of rolling assisted biaxially textured substrates (RABiTS) and epitaxial deposition or formation of HTS on such substrates is reported. Significant progress has been made in understanding the role of meso-scale defects such as grain boundaries on long-range current flow of HTS conductors made using the RABiTS approach. Both experimental and theoretical calculations suggest that in well-textured samples these commonly present defects do not provide an intrinsic barrier to current flow in long-length conductors. Significant progress has also been made in the reel-to-reel deposition of oxide buffer layers and in the fabrication of long-length superconductors using the ex situ BaF₂ technique. Finally, non-magnetic, mechanically strengthened, biaxially textured metal templates have been fabricated with high quality oxide buffer layers. Epitaxial formation of YBCO on such substrates yields critical current densities over 1 MA/cm² at 77 K, 0 T. Published by Elsevier Science B.V.

1. Introduction

High critical current density conductors fabricated by epitaxial deposition of high temperature superconductors on rolling assisted biaxially textured substrates (RABiTS) has been suggested as a possible route towards realizing low cost, high

performance superconducting wires for a variety of applications [1–3]. In this process, a well-formed cube texture is first developed in a metal/alloy template, followed by epitaxial deposition of intermediate oxide buffer layers and superconductors. In this paper, we first discuss the nature of this textured template in order to examine fundamental limitations towards the fabrication of high- J_c conductors on such templates. Next, advances made in the continuous processing of longer length RABiTS and epitaxial YBCO on RABiTS are summarized. Finally, recent progress made in the

* Corresponding author. Tel.: +1-423-574-1587; fax: +1-423-574-7659.

E-mail addresses: goyala@ornl.gov, zag@ornl.gov (A. Goyal).

fabrication of substrates with reduced magnetism and increased mechanical strength and in depositing high quality epitaxial oxide buffer layers and YBCO on such substrates, is presented.

2. Results and discussion

2.1. Fundamental issues affecting J_c of YBCO on RABiTS

Fundamental issues affecting the critical current density of epitaxial, high temperature superconductors on RABiTS were examined. First, GBs in RABiTS are examined using electron backscatter Kikuchi diffraction. Second, issues related to percolative pinch-off of the critical current density for long conductors due to a large grain size in the substrate and a finite width of the substrate are addressed. Third, texture stability and homogeneity in long-length substrates is discussed. Lastly, the effect of GB grooving in the metal substrate and its affect on the critical density is examined.

2.1.1. Grain boundaries in RABiTS

Extensive examination of GBs in the textured metal substrate and the YBCO layer was performed using electron backscatter Kikuchi diffraction [4]. Data was gathered on a hexagonal grid at a spacing of $\sim 3 \mu\text{m}$. At each point, indexing of the backscatter diffraction pattern gave a unique measure of the orientation of the sample. Using such a technique, all GBs present in the sample in the area examined are revealed. Fig. 1 shows a set of GBs maps obtained from a $0.5 \times 0.5 \text{ mm}^2$ area of a textured Ni substrate. Contrast in the image is that produced by electron backscatter pattern quality and may be related to channeling effects [4]. Grain boundary (GB) maps are drawn such that all boundaries greater than a certain angle are shown in the panel in question. For example, in the first micrograph all GBs greater than 1° are shown. This criterion is then progressively increased for each panel. As can be seen from the GB map with boundaries greater than 5° , most of the substrate is percolatively connected. Few boundaries are observed in maps showing GBs greater than $5\text{--}6^\circ$. Hence, these substrates are

reasonably well textured, although further shifting of the GB angles to lower misorientations would be desirable.

On depositing epitaxial YBCO with intermediate oxide buffer layers on such Ni substrates, excellent epitaxy is observed in the plane of the substrate [5]. However, a significant improvement is observed in the out-of-plane texture [5]. This improvement can be as high as 5° for films deposited on the YSZ surface on Ni, and between 3° and 5° for films deposited on the CeO_2 surface on Ni. Hence, the GB misorientations in the YBCO layer have to necessarily be somewhat lower than the corresponding GB misorientations in the Ni substrate below. It is important to note that GB misorientations shown in Fig. 1, reflect the total misorientation at the boundary, i.e. both in-plane and out-of-plane. Several YBCO films on RABiTS were also examined in detail using electron backscatter diffraction. In all cases it was found that there were few GBs with misorientations greater than 5° . Examination of YBCO films on different Ni substrates indicates that the typical cross-section of the film connected with boundaries greater than 5° is between 5% and 10% depending on the completeness of cube texture formation in the substrate. Clearly, upon improving the texture further, this small fraction of higher angle GBs can be minimized.

The data shown in Fig. 1 were obtained from a Ni substrate which was $125 \mu\text{m}$ thick. Typically after the cube texture formation is complete, the average grain size in the substrate approaches the thickness of the substrate, in this case being $\sim 125 \mu\text{m}$. However, typical thickness of substrates currently used for RABiTS fabrication is $50 \mu\text{m}$. The average grain size of these substrates, as expected, is found to be $\sim 50 \mu\text{m}$. This change to thinner substrates was made with the objective of obtaining conductors with higher engineering critical current densities as well as minimizing material costs. Typical Ni tapes currently used are 1 cm in width, and with an average grain size of $50 \mu\text{m}$, are essentially 200 grains wide. Because of this large grain size in the substrate relative to the width of the substrate, it is important to examine if this may result in a percolative pinch-off by higher angle GBs in the substrate if one were to fabricate very

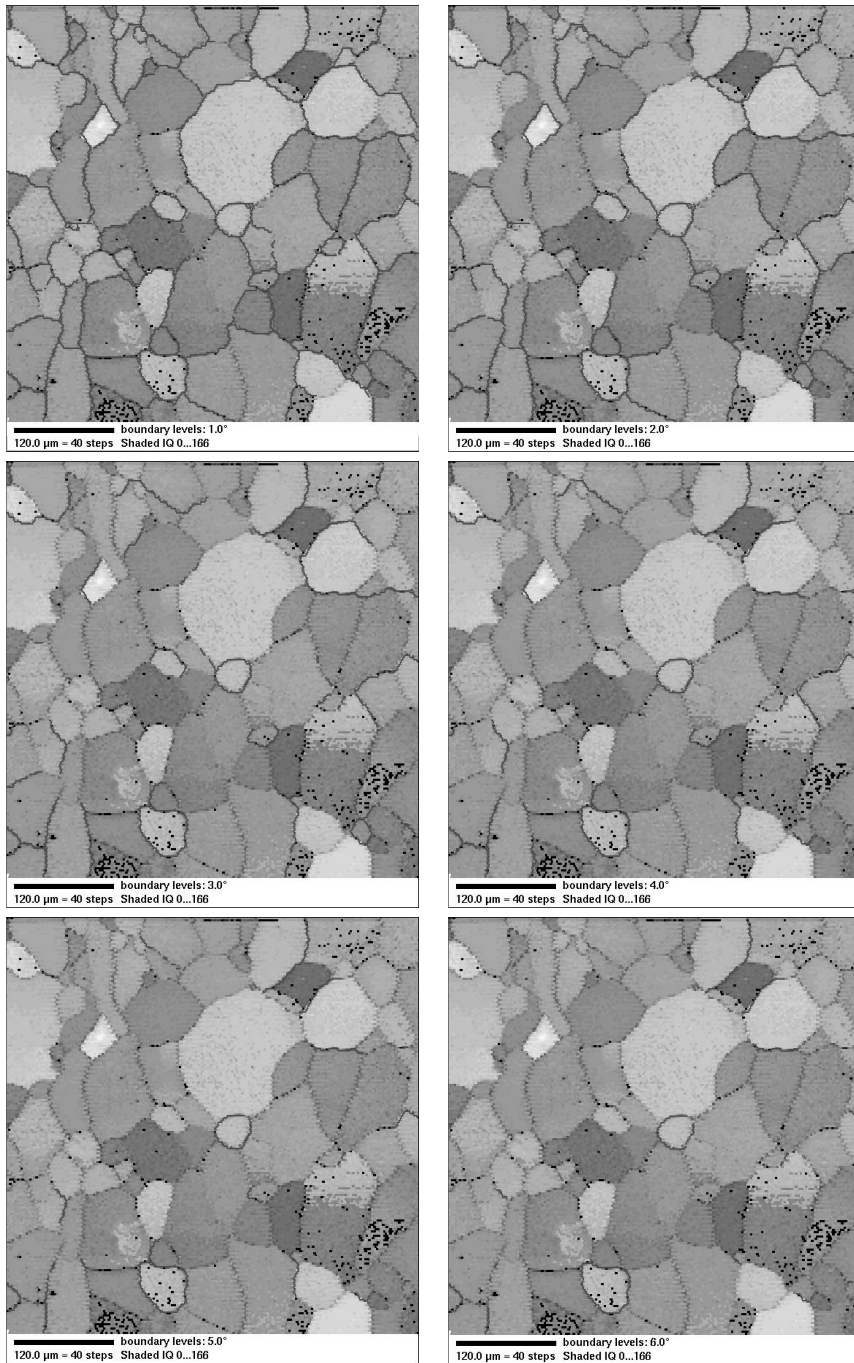


Fig. 1. GB maps of a $0.5 \times 0.5 \text{ mm}^2$ region of a textured Ni substrate. GB maps are drawn such that all boundaries greater than a certain angle are shown in the panel in question. For example, in the first micrograph all GBs greater than 1° are shown. This criterion is then progressively increased for each panel. As can be seen from the GB map with boundaries greater than 5° , most of the substrate is percolatively connected. Few boundaries are observed in maps showing GBs greater than $5\text{--}6^\circ$.

long conductors. This issue was studied by performing limiting path calculations [6] of J_c as a function of the width of the substrate relative to the average grain size for long substrates and is presented in the following section.

2.1.2. Effect of large grain size of the metal substrate and the finite width of the substrate

Limiting path calculations based on the technique proposed by Rhyner and Blatter [6] were performed [7]. As opposed to square lattice, a more realistic hexagonal lattice of grains was assumed. GBs were randomly assigned to be conducting or non-conducting based on a total fraction, f , of conducting GBs. The total fraction, f , of conducting GBs is related to the macroscopic texture of the textured metal template based on a certain dependence of J_c on misorientation angle. For example, a sample with a full-width-half-maximum (FWHM), ϕ , the expected grain boundary misorientation distribution (GBMD) is also Gaussian and has a FWHM of $\sqrt{2}\phi$. We further assume that GBs with misorientations greater than 5° carry no current, i.e. are non-conducting, and those with misorientations below 5° , have J_c similar to the intra-granular J_c and are conducting. Based on this dependence of J_c with misorientation angle and the FWHM of the GBMD, the fraction, f , of conducting GBs can be deduced [7]. The sample J_c is normalized so that $J_c = 1$ when all boundaries are conducting. Sample length and width are measured in units of grains. In order to eliminate end effects, periodic boundary conditions are applied in the direction of current flow [7].

In order to find J_c for a range of sample lengths, J_c was calculated for 20,000 samples, each 1000 grains long. Thus the total length sampled is 2×10^7 grains. For a typical RABiTS substrate the average grain size is $50 \mu\text{m}$, so the length sampled is ~ 1 km. Sample widths of 10, 20, 50, 100 and 200 grains were considered.

Fig. 2 shows the calculated J_c for a 1 km long RABiTS substrate with epitaxial HTS versus the width of the conductor as a function of the macroscopic texture [7]. As indicated in the figure, reductions in J_c due to the finite width of the substrate become negligible for a width of the conductor greater than 100 grains. Typical RABiT

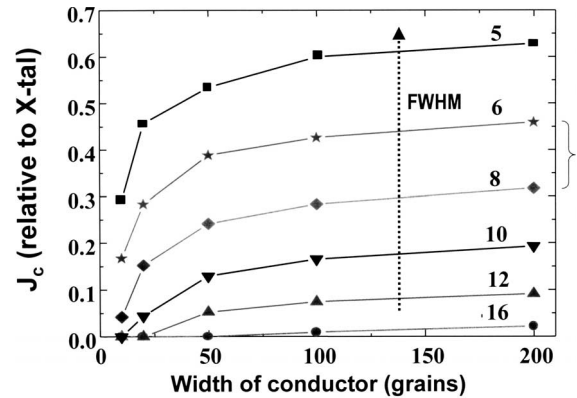


Fig. 2. Minimum J_c relative to that of single crystal YBCO for 20,000 samples each 1000 grains long (for a typical RABiTS Ni, the grain size is $50 \mu\text{m}$, so this results in a sampling of ~ 1 km long wire), as a function of the width of the conductor in units of grains. The different curves correspond to conductors with different FWHM of the macroscopic texture. The bracket corresponds to where typical RABiTS lie on this plot. Most long-length Ni fabricated so far have a FWHM of 8° .

substrates are 1 cm wide or 200 grains wide. Hence percolative pinch-off of J_c due to a large grain size in the substrate and a finite width of the substrate is *not* an issue for fabricating long-length, epitaxial HTS conductors based on the RABiTS technique.

Another important finding can be inferred from Fig. 2. Typical long-length RABiT substrates have a texture corresponding to a FWHM of ~ 6 – 8° , and more often are closer to 8° than 6° . For a 200 grains wide conductor, Fig. 2 indicates that the expected J_c is about ~ 0.3 (single crystal J_c) for a typical substrate with a FWHM of 8° . Fig. 2 further indicates that if the texture of the substrates can be improved to obtain a FWHM of 6° or 5° , then a corresponding factor of 1.5 or 2 enhancement in J_c may be possible.

2.1.3. Texture homogeneity in long-length thermomechanically processed metal substrates

Fig. 3 shows a continuous measurement of the (200) and (111) peak intensities for a 20 m long textured Ni substrate. The figure indicates that the (200) peak intensity is essentially constant along the 20 m length. The (111) peak intensity at all points is below the background indicating a fully

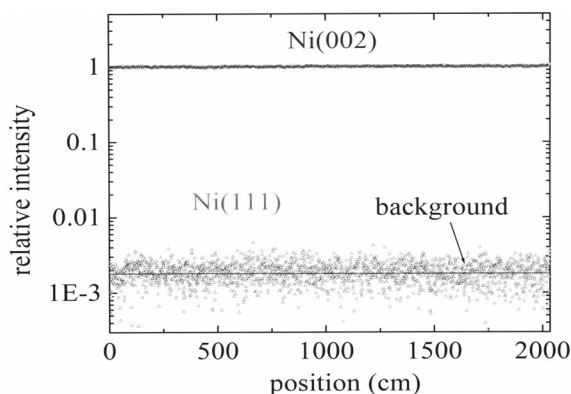


Fig. 3. (002) and (111) X-ray peak intensities measured continuously along the length of a 20 m long cube-textured Ni substrate, 1 cm wide and 50 μm thick. As can be seen, the (002) peak intensity is essentially constant along the length. The (111) peak intensity at all points is below the average background intensity.

formed cube texture with no secondary textures or twins. Measurement of the in-plane and out-of-plane texture as a function of the length of the conductor, show that the FWHM of the conductor is also constant along the length with relatively little fluctuation. Hence the expected GBMDs along the length of the tape are also expected to be constant. Since excellent texture homogeneity can be obtained in long-lengths of Ni, texture inhomogeneity is not a limiting factor towards fabricating long-lengths of high- J_c epitaxial YBCO on RABiTS.

Long-lengths of such Ni substrates have been fabricated. Fig. 4 shows ~ 2 km long, rolled Ni substrates, 1 cm wide and 50 μm thick, which upon annealing give textures similar to that shown in Fig. 3.

2.1.4. Effect of thermal grooving in metal substrate on J_c

In order to determine the thermal groove characteristics in textured metal substrates, atomic force microscopy (AFM) was used to characterize the thermal groove profiles of 300 GBs in Ni substrates annealed at 800°C for 10–120 min. Fig. 5 shows a typical AFM scan on a triple point of Ni. It can be seen that the extent of GB grooving in the three boundaries at the triple point is dif-

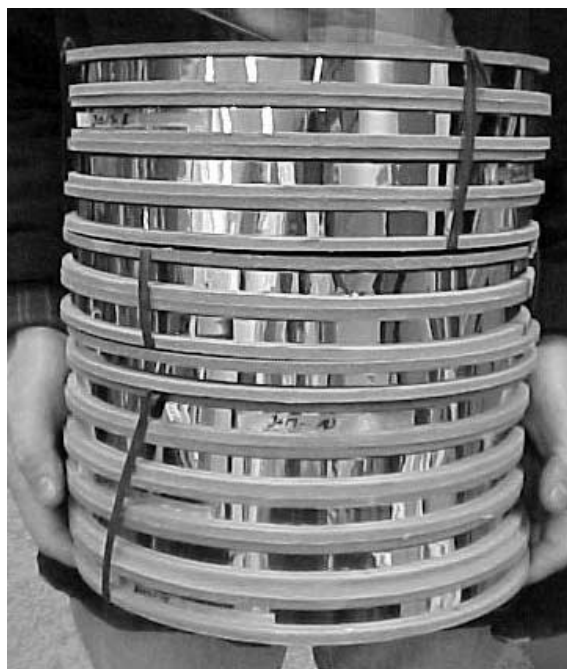


Fig. 4. 2 km of Ni, 1 cm wide and 50 μm thick has been fabricated which upon annealing at 1100°C for 1 h yields textures similar to those shown in Fig. 5. ω - and ϕ -scans of oxide multilayers deposited epitaxially on a Ni-7 at.%Cr substrate by pulsed laser ablation.

ferent. In order to correlate GB grooving with GB misorientation as well, electron backscatter Kikuchi diffraction was used to obtain the misorientation of all GBs characterized by AFM for groove profiles.

In general, the thermal groove depth and width increased with the annealing time at 800°C. The results obtained are summarized below in Table 1. Correlation of groove depth and width with the GB misorientation angle showed that in general with increasing misorientation angle, both the GB depth and the width increased [8]. However, considerable scatter in data suggests that perhaps GB plane may also be playing a significant role [8].

These results imply that under typical annealing conditions, GB grooves in Ni are very shallow and wide with large dihedral angles. In order to examine the effect of such grooves on J_c in the YBCO layer, four Ni substrates were annealed at 800°C for 120 min (the annealing condition which results

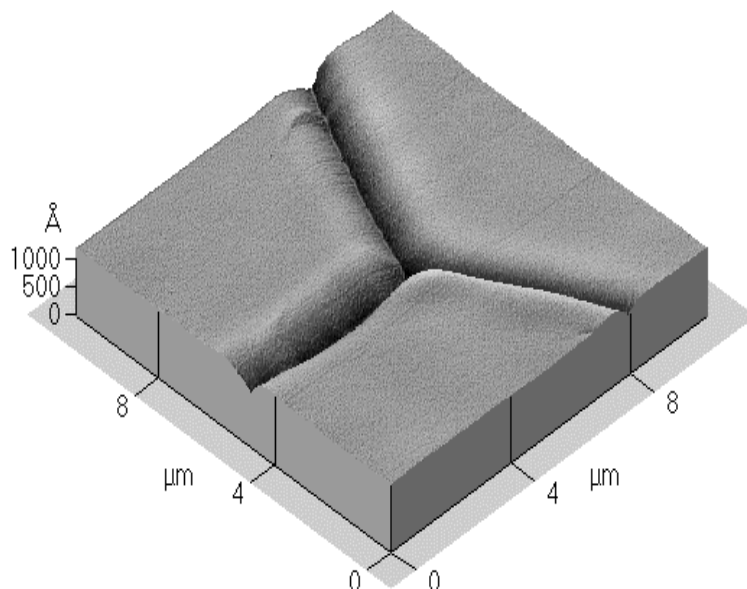


Fig. 5. Typical AFM image of a triple point in annealed Ni. Evidence of thermal grooving at the three GBs can be seen.

Table 1

Summary of thermal groove characteristics in Ni for samples annealed at 800°C for 10–120 min

Characteristic	Range observed
Width	1.25–1.70 μm
Depth	175–290 Å
Dihedral angle	175–179°

in the deepest grooves). Oxide buffer layers of configuration CeO₂/YSZ/CeO₂ were then deposited epitaxially, followed by formation of epitaxial YBCO using the ex situ BaF₂ process [3,9]. In each case, J_c (0 T, 77 K) was found to be greater than 2 MA/cm² [8]. Moreover, the field dependence is similar to that obtained for YBCO films on single crystal substrates [8]. These results imply that GB grooving in the metal substrate does not adversely affect J_c .

2.2. Long length oxide buffer layer deposition and YBCO on such substrates using the ex situ BaF₂ process

Scaling of the RABiTS process from fabrication of a short, stationary sample to a longer sample

fabricated by continuous motion of the sample at all steps, requires significant modification of the processing equipment. This is because reel-to-reel handling and processing is necessary at all steps. At the Oak Ridge National Laboratory, we have adopted a modular approach wherein almost all steps in the process are broken down into separate reel-to-reel systems. Fig. 6 shows a flow diagram for the processing of longer length samples by continuous reel-to-reel processing. As indicated in the figure, a number of reel-to-reel systems are required. This modular approach was adopted because it allows for independent optimization at each step without the complications of cross-talk at any stage.

High quality, epitaxial oxide layers have been successfully deposited in a reel-to-reel configuration. Typically, the first CeO₂ is layer deposited by e-beam evaporation [10]. Conditions under which is this is performed have been reported previously by Cui et al. [10]. The remaining two oxide buffer layers are deposited using RF sputtering in a separate reel-to-reel system [11]. Y–BaF₂–Cu precursor films are then co-evaporated in another reel-to-reel system [12]. Rutherford backscattering spectrum (RBS) measurements indicate that an

Start with spools of custom rolled metal tape in long lengths



Clean tape ultrasonically to remove debris and organics



Anneal tape to develop texture



← XRD

Grow CeO_2 seed layer by e-beam



← XRD

Grow YSZ and CeO_2 layers by sputtering



← XRD

Deposit YBCO precursor



React precursor to form YBCO



← XRD

Overcoat YBCO with silver.



Measure I_c / J_c .

average composition of Y/Ba/Cu : 1.05/2.10/3.0 with a standard deviation of less than 2% can be obtained [12]. Moreover, thickness variations of such precursor films is less than 2.5% over lengths up to one meter [12].

A separate reel-to-reel precursor conversion system for forming YBCO ex situ has also been established [11]. This is essentially a furnace with take-off and pay-out reels on either ends. The critical part of the furnace design involves optimization of the gas flow profiles. This is yet to be completely optimized.

The best meter long superconducting tape obtained by conversion from this reel-to-reel furnace showed a J_c of 100,000 A/cm² end-to-end using a 1 $\mu\text{V}/\text{cm}$ criterion at 77 K and self-field [11,12]. Examination of the J_c of every 1 cm long segment of the tape indicated that except one segment, every segment had a J_c between 300 and 750 kA/cm² [11]. It is speculated that in this low- J_c segment, contamination of the substrate occurred prior to the YBCO precursor deposition. This indication comes from X-ray measurements which reveal that while the oxide buffer layers in this segment had the same texture as elsewhere in the substrate, non-epitaxial YBCO was present in this segment. J_c fluctuations in the remainder of the tape correlated very well with the intensity fluctuations of the YBCO (005) peak. This in turn correlated well with some unreacted precursor material on the surface of the tape across the width of the substrate [11]. Efforts are currently underway to further optimize the conversion conditions both by modification of the processing conditions as well as by modification of the furnace design.

2.3. Reduced magnetism, strengthened substrates

Ni–Cr alloy substrates with Cr contents upto 13 at.%Cr were fabricated by rolling to deformations greater than 95% followed by annealing at high temperatures to form cube textured alloy tapes [13]. As expected, it is found that the Curie temperature decreases linearly with Cr addition. Measured Curie temperatures for alloys studied are summarized in the Table 2. Also indicated in Table 2 are measured yield strengths for the alloys. Tensile tests were performed on cube textured,

Fig. 6. Flow diagram for fabrication of longer YBCO on RABiTS by continuous processing at all steps in a reel-to-reel configuration.

Table 2
Measured Curie temperatures and tensile yield strength for Ni-Cr alloys

Composition	Curie temperature (K)	Yield strength (MPa)
Ni	627	34
Ni-7 at.%Cr	250	64
Ni-9 at.%Cr	124	87
Ni-11 at.%Cr	20	102
Ni-13 at.%Cr	0	164

laser machined, dog-bone samples with the stress applied along the [1 0 0] crystallographic axis.

As can be seen from Table 2, Ni-13 at.%Cr alloys are essentially non-magnetic whereas Ni-7 at.%Cr alloys have a Curie temperature only slightly below room temperature. For applications

above 40 K, both Ni-11 at.%Cr and Ni-13 at.%Cr would be non-magnetic. With increase in Cr additions, the yield strength increases substantially with the Ni-13 at.%Cr substrate having a strength almost a factor of five times that of pure Ni.

For alloys with low Cr contents, epitaxial oxide buffer layers can be deposited directly on the substrate under conditions similar to that developed for deposition on Ni. Fig. 7 shows ϕ - and ω -scans of oxide multilayers deposited epitaxially on a Ni-7 at.%Cr substrate by pulsed laser ablation. The microstructure of the YBCO layer on the top is shown in Fig. 8. The scanning electron micrograph shows that the film is relatively dense and crack free. The critical current density of this YBCO film was 223,000 A/cm² at 77 K and 0 T.

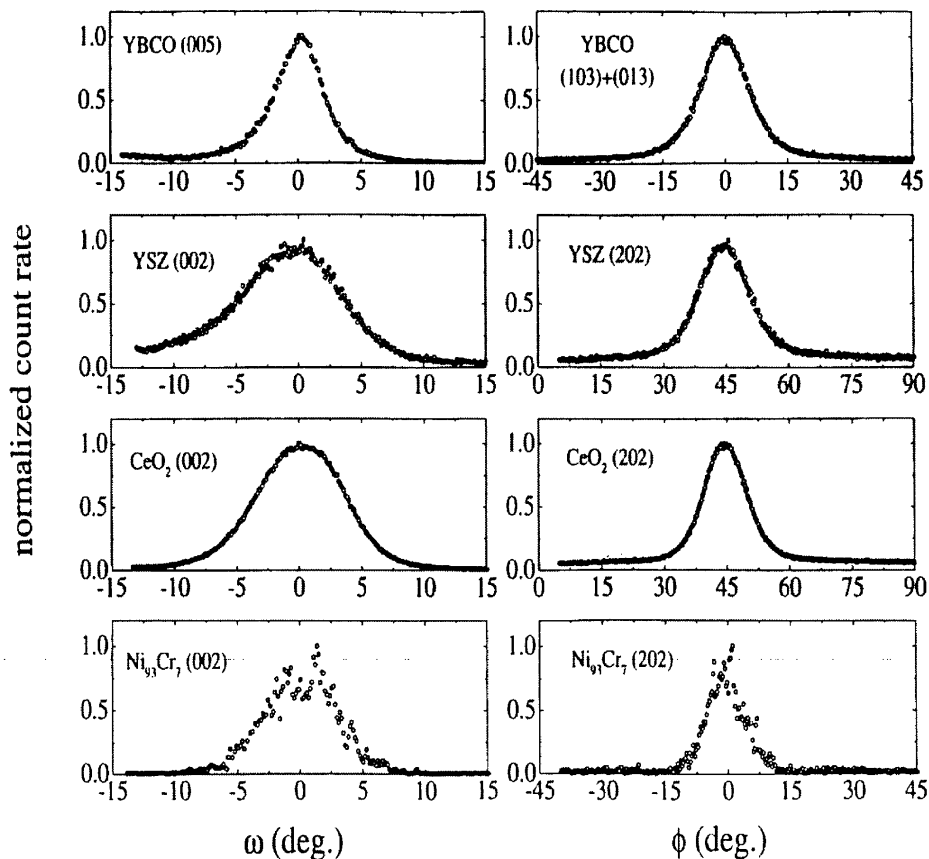


Fig. 7. ω - and ϕ -scans of oxide multilayers deposited epitaxially on a Ni-7 at.%Cr substrate by pulsed laser ablation.

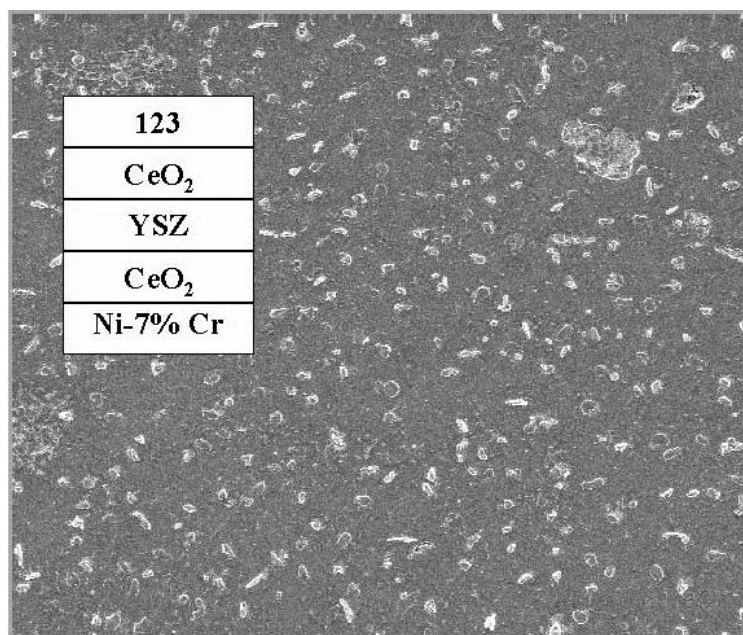


Fig. 8. Scanning electron micrograph of the YBCO surface on a biaxially textured Ni-7 at.%Cr substrate.

Even though, relatively good epitaxy is obtained in a significant part of the substrate, it is expected that localized oxidation and formation of chromium oxide is a problem. This issue becomes significant for higher chromium content substrates. Typically, the deposition of oxide layers on biaxially textured Ni is performed under conditions such that the formation of NiO is thermodynamically unstable, whereas the formation of the oxide layer in question such as CeO₂ is thermodynamically stable. For example, during electron beam evaporation of Ce to form high quality, epitaxial CeO₂ on Ni, careful control of the partial pressures of H₂, H₂O and O₂ is essential [10,14–16]. The partial pressure of O₂ is kept to a minimum and the partial pressure of H₂O is monitored to provide sufficient oxidation of Ce to form stoichiometric CeO₂ [10,14–16]. NiO formation is not thermodynamically favorable under a wide range of H₂O partial pressures, whereas formation of CeO₂ is thermodynamically stable. Similar thermodynamic considerations show that under typical conditions for epitaxial deposition of CeO₂ on Ni, formation of chromium oxide is also thermodynamically expected.

In order to minimize the deleterious effects of chromium oxide formation, an additional step was introduced [17]. By first depositing an epitaxial layer of Ni on the Ni–Cr substrates, the surface for epitaxy of the first oxide layer is not exposed to the Ni–Cr surface. Hence, deposition of oxide layers can now be done under the same conditions developed for deposition of Ni. Furthermore, after the oxide layer depositions, the Ni layer initially deposited is now diffused into the substrate. Hence this Ni layer can be considered to be transient.

Fig. 9 shows RBS of a fully buffered Ni-13 at.%Cr substrate. The first CeO₂ layer was deposited using electron beam evaporation using conditions described elsewhere [15] and the top two layers were deposited using RF sputtering using conditions described by List et al. [16]. The various peaks observed and the layer they correspond to are indicated in the figure. All layers have a relatively sharp interface implying negligible inter-diffusion. Also shown in the figure is the RBS spectra obtained from the substrate after an O₂ anneal at 500°C for 1 h. The 500°C anneal in flowing O₂ is a rather harsh anneal but useful to see how the substrate would hold up under such

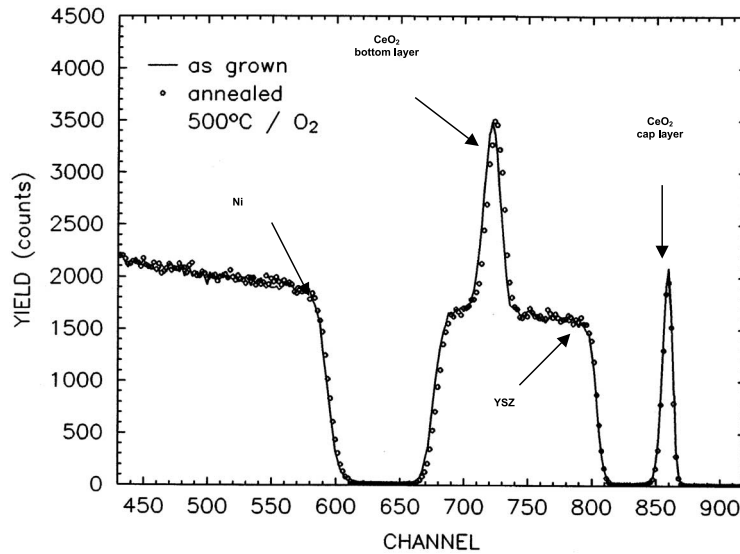


Fig. 9. RBS of a $\text{CeO}_2/\text{YSZ}/\text{CeO}_2/\text{Ni-13 at.}\% \text{Cr}$ substrate. The solid line is for the as deposited RABiT substrate and the points are for the same substrate after an anneal in flowing O_2 at 500°C for 1 h.

conditions. As can be seen, the RBS spectra is hardly affected after the anneal.

YBCO films were then fabricated on this substrate by using the two step, ex situ BaF_2 method [9]. Excellent epitaxy of the YBCO film was obtained with the out-of-plane texture showing a significant improvement in the FWHM [8]. The YBCO film had a critical current density of $1.4 \text{ MA}/\text{cm}^2$ at 77 K, self-field. Moreover the field dependence of J_c was similar to that observed for typical YBCO on RABiTS [8].

3. Summary

Fundamental issues affecting the critical current density of epitaxial, high temperature superconductors on RABiTS were studied. Examination of GBs in the textured Ni and the YBCO layer performed using electron backscatter Kikuchi diffraction shows that in high- J_c samples there is only a small cross-section of the sample connected by GBs with misorientations larger than 5° . Clearly, upon improving the texture further, this small fraction of higher angle GBs can be further minimized.

Limiting path calculations show that percolative pinch-off of the critical current density for long conductors due to a large grain size in the substrate and a finite width of the substrate is not an issue for conductors greater than 100 grains wide. The calculations also show that only a few degree improvement in the in-plane texture of the substrates could result in significant enhancements in J_c .

The texture stability and homogeneity in long-length substrates was found to be excellent. Measurement of texture along the length of a 20 m long Ni tape shows negligible fluctuations in the texture. Hence, texture inhomogeneity in long substrates is not an intrinsic limiting factor in obtaining long, high- J_c tapes. Upto $\sim 2 \text{ km}$ of well-textured Ni tapes have been fabricated. Characterization of 300 GB grooves in annealed, cube-textured Ni substrates shows that the typical grooves in Ni have large dihedral angles. The grooves are also highly aspected with the widths being significantly larger than the depths. Even for Ni substrates with very well-formed GB grooves, no degradation of J_c was observed. Hence, GB grooving is not expected to be limiting factor towards fabricating long, high- J_c tapes based on the RABiTS approach.

Several reel-to-reel systems have been established to facilitate continuous fabrication of RABiTS and YBCO on RABiTS. Observed variations of J_c in meter long YBCO on RABiTS are attributed to handling issues and incomplete YBCO formation rather than any identifiable fundamental limitation.

Lastly, Ni–Cr substrates with well-developed cube textures, reduced magnetism and increased mechanical strength were fabricated. Ni-13 at.%Cr substrates are essentially non-magnetic to temperatures as low as 4.2 K and have yield strengths a factor 5 higher than that of pure Ni. High quality oxide buffer layers have been successfully deposited on these substrates. High quality epitaxial YBCO films fabricated on oxide buffered alloy substrates using the ex situ, BaF_2 process. A high critical current density (1.4 MA/cm²) has been demonstrated on the non-magnetic, Ni-13 at.%Cr alloy substrate.

Acknowledgements

Research sponsored by US Department of Energy, Office of Energy Efficiency and Renewable Energy, Office of Power Technologies, Superconductivity Program under contract DE-AC05-96OR22464 to UT-Battelle LLC.

References

- [1] A. Goyal, D.P. Norton, J.D. Budai, M. Paranthaman, E.D. Specht, D.M. Kroeger, D.K. Christen, Q. He, B. Saffian, F.A. List, D.F. Lee, P.M. Martin, C.E. Klabunde, E. Hatfield, V.K. Sikka, *Appl. Phys. Lett.* 69 (1996) 1795.
- [2] A. Goyal, J. Budai, D.M. Kroeger, D. Norton, E.D. Specht, D.K. Christen, US Patents: 5, 739, 086; 5, 741, 377; 5, 898, 020; 5, 958, 599.
- [3] A. Goyal, R. Feenstra, F.A. List, M. Paranthaman, D.F. Lee, D.M. Kroeger, D.B. Beach, J.S. Morrell, T.G. Chirayil, D.T. Verebelyi, X. Cui, E.D. Specht, D.K. Christen, P.M. Martin, *JOM* 51 (1999) 19.
- [4] A. Goyal, S.X. Ren, E.D. Specht, D.M. Kroeger, R. Feenstra, D.P. Norton, M. Paranthaman, D.F. Lee, D.K. Christen, *Micron* 30 (1999) 463.
- [5] A. Goyal, D.P. Norton, D.M. Kroeger, D.K. Christen, M. Paranthaman, E.D. Specht, J.D. Budai, Q. He, B. Saffian, F.A. List, D.F. Lee, E. Hatfield, P.M. Martin, C.E. Clabunde, J. Matthis, C. Park, *J. Mater. Res.* 12 (1997) 2924.
- [6] J. Rhyner, G. Blatter, *Phys. Rev. B* 40 (1989) 829.
- [7] E.D. Specht, A. Goyal, D.M. Kroeger, *Supercond. Sci. Tech.* 13 (2000) 592.
- [8] A. Goyal et al., in preparation.
- [9] R. Feenstra, T.B. Lindemer, J.D. Budai, M.D. Galloway, *J. Appl. Phys.* 69 (1991) 6569.
- [10] X. Cui, F.A. List, D.M. Kroeger, A. Goyal, D.F. Lee, J. Mathis, E.D. Specht, P.M. Martin, R. Feenstra, D.T. Verebelyi, D.K. Christen, M. Paranthaman, *Physica C* 316 (1999) 27.
- [11] D.F. Lee et al., in preparation.
- [12] S.W. Lu, F.A. List, D.F. Lee, X. Cui, M. Paranthaman, B.W. Kang, D.M. Kroeger, A. Goyal, P.M. Martin, R.E. Ericson, *Thin Solid Films*, submitted for publication.
- [13] A. Goyal, E.D. Specht, D.M. Kroeger, M. Paranthaman, US patent 5964966.
- [14] Q. He, D.K. Christen, J.D. Budai, E.D. Specht, D.F. Lee, A. Goyal, D.P. Norton, M. Paranthaman, F.A. List, D.M. Kroeger, *Physica C* 275 (1997) 155.
- [15] M. Paranthaman, A. Goyal, F.A. List, E.D. Specht, D.F. Lee, P.M. Martin, Q. He, D.K. Christen, D.P. Norton, J.D. Budai, D.M. Kroeger, *Physica C* 275 (1997) 266.
- [16] F.A. List, A. Goyal, M. Paranthaman, D.P. Norton, E.D. Specht, D.F. Lee, D.M. Kroeger, *Physica C* 302 (1998) 87.
- [17] A. Goyal, D.M. Kroeger, M. Paranthaman, D.F. Lee, R. Feenstra, D. Norton, US patent pending.